Quantitative Multi-Agent Models for Simulating Protein Release from PLGA Bioerodible Nano- and Microspheres

Ana Barat[*1], Martin Crane[2] and Heather J. Ruskin[3]

[1] Modelling and Scientific Group, Faculty of Engineering and Computing, School of Computing, Dublin City University, Dublin 9, Ireland, Tel. +353 1 700 5661, email: `abarat@computing.dcu.ie`

[2] `mcrane@computing.dcu.ie`

[3] `hruskin@computing.dcu.ie`

Summary. Using poly(lactide-co-glycolide) (PLGA) particles for drug encapsulation and delivery has recently gained considerable popularity for a number of reasons. An advantage in one sense, but a drawback of PLGA use in another, is that drug delivery systems made of this material can provide a wide range of dissolution profiles, due to their internal structure and properties related to particles' manufacture. The advantages of enriching particulate drug design experimentation with computer models, are evident with simulations used to predict and optimize design, as well as indicate choice of best manufacturing parameters. In the present work, we seek to understand the phenomena observed for PLGA micro- and nanospheres, through Cellular Automata (CA) agent-based Monte Carlo (MC) models. Systems are studied both over large temporal scales, (capturing slow erosion of PLGA) and for various spatial configurations (capturing initial as well as dynamic morphology). The major strength of this multi-agent approach is to observe dissolution directly, by monitoring the emergent behaviour: the dissolution profile manifested, as a sphere erodes. Different problematic aspects of the modelling process are discussed in details in this paper. The models were tested on experimental data from literature, demonstrating very good performance. Quantitative discussion is provided throughout the text in order to make a demonstration of the use in practice of the proposed model.

Keywords: drug delivery, PLGA, microspheres, nanospheres, dissolution, modelling, multi-agents, simulation, Monte Carlo, Cellular Automata.

1 Introduction

Nano- and microspheres are particulate drug delivery systems (DDS) of nanometer or micron size ranges respectively, consisting of bioerodible solids, which can incorporate therapeutic agents, such as small drugs or macromolecules [1]. During the last decades, particulates have evolved from an alternative experimental type of sustained delivery to a prominent class of DDS with various applications and many promising future developments [2]. Currently, polymeric particulates have found applications in many key bioengineering fields such as: bone repair, tissue engineering and development [1, 3, 4], and biomedical applications like vaccine delivery, various treatments for cancer, AIDS, tuberculosis and other diseases [5, 6, 7, 8].

One of the most successful polymers, used in the production of particulates for controlled release is PLGA. An advantage of this polymer is that biocompatible and biodegradable products of dissolution of the particles do not require further manipulation after introduction to the body. Besides the fact that it is non-toxic (PLGA nanospheres can be 16 times more effective for cell viability than the free drug, [5]), this material has proved capable of easy encapsulation [5] and subsequent release of drug (especially of pharmaceutically active proteins), in a sustained manner. Experimental studies such as [5, 9, 10] demonstrate the potential for encapsulation and sustained release of a wide variety of proteins from PLGA spheres.

PLGA belongs to the group of bulk eroding polymers. These polymers erode slowly and water uptake by the system is much faster than polymer degradation. In this case, erosion is not restricted to the polymer surface, because the entire system is rapidly hydrated and polymer chains are cleaved throughout the device [11]. This mechanism permits using PLGA in controlled-release applications.

Another reason for the success of PLGA in particle manufacture is the versatility of its release properties, which can be modified by varying composition (lactide/glycolide ratio), molecular weight and chemical structure. In this way, a wide range of *in vivo* life-times of PLGA can be obtained: from three weeks to over a year [1]. On the other hand, release profiles are also significantly influenced by the method of microencapsulation [1, 3], because the latter is at the origin of obtaining one or another internal morphology of the particles. While one method results in the protein solid dispersion within the polymeric matrix (Figure 1, (a)), others yield structures where the protein can be located in the occlusions and large pores, formed during the production of spheres [1], Figure 1, (b). With the downside that total control of the pore sizes is still not possible, some studies, such as [3], mention good results such as control over the order of pore dimension.
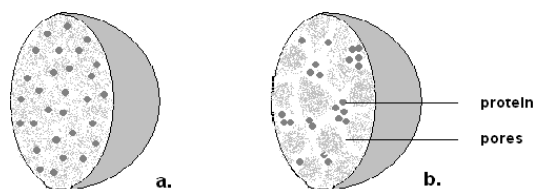

Fig. 1. a) Sphere morphology obtained by the solid-in-oil-in-water solvent evaporation technique. b) Sphere morphology obtained by water- in-oil-in-water solvent evaporation technique. Adapted from [1].

To date, the biomedical potential of polymeric particulate formulations is far from being fully explored [2]: the area is growing and expanding, but not as rapidly as it has potential for. Applications require concomitantly highly specific, nontoxic and functional solutions, characterised by delivery times ranging from weeks to months, which make experimental research in particulates extremely time- and resource-intensive. In this context, complementing exper-

imentation with modelling and simulation can be both a scientific challenge and an economically viable solution. There are currently few reports dealing with investigation of different modelling techniques for protein dissolution from PLGA spheres. Most adapt differential equation methods to describe the concentrations of diffusing molecular species at different space and time points [12, 13, 14]. Continuous and homogeneous morphology-related variables are required to establish grids for solving the partial differential equations numerically. However, as noted, the particle environment is usually discrete and heterogeneous. In order to adapt to the porous environment of microspheres, (which depends on initial porosity and its time-dependent growth), methods use estimates for global parameters such as porosity (ϵ) and tortuosity (τ), which ultimately affect drug diffusion coefficient D, e.g. [12, 14].

A break through in modelling the increased complexity in the drug delivery field was achieved by the class of Cellular Automata (CA) and Monte Carlo (MC) based microscopic models. In early work of Göpferich and Zygourakis [4, 15, 16, 17, 18], the polymer, together with the dissolution medium around it, is represented as a probabilistic cellular automaton: the DDS is mapped on a computational grid of discrete sites filled with polymer, which degrades according to a set of rules. Subsequently, [12] Siepmann et al. proposed a partial differential equation model, coupled with a MC simulator. Although sounding very promising, the authors' feeling is the CA and MC models have not been exploited to their full potential in the area.

Almost all known modelling approaches available [11, 12, 14] consider *homogeneous* distributions of the pores and of proteins in the spheres, experiments have indicated that this may not realistically describe the majority of cases [9, 19], with internal configuration of the spheres subject to *heterogeneity*.

[9] reveals that spheres enclosing smaller proteins appear to have an open branched network throughout. However, those enclosing larger proteins have pores in the outer layers and appeared open near the surface, while having a more dense structure in the inner layers of the sphere.
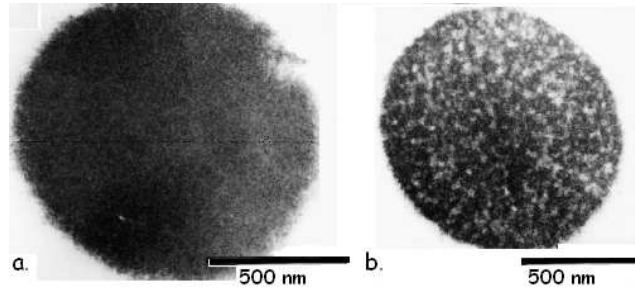

Fig. 2.   a) Control PLGA sphere, no encapsulated molecules b) PLGA sphere encapsulating carbonic anhydrase, adapted from [9].

In further discussion of microspheres properties, [13] assumes that adsorption of macromolecules to the surface of the microsphere (or to the large occlusions inside the spheres), suggesting an *uneven distribution* of the macromolecule in the volume of the sphere.

Even if the internal morphology of the spheres was showed to be heterogeneous and to influence the final dissolution profile, no CA and MC modelling work, specifically taking it into consideration has, to the author's knowledge, previously been reported.

In the present paper, we depart from the idea that, for dissolution of proteins from PLGA delivery systems, both pre-existent and dynamically formed pores influence directly the resulting release profile. Hence, the aim was to *simulate explicitly and simultaneously* both PLGA erosion and protein dissolution process. The innovative features of this work, the authors believe, lie in the following: multiple agents to model both protein and their PLGA en-

vironment, very fine-grained modelling of the spheres, using complementary data to model the spheres' 3D internal morphologies and an user-accessible quantitative calibration.

2 Modelling

The dimensions of the experimental entities involved range from several nanometers (proteins) to several microns (spheres). A comparatively simple protein example like the lysozyme (13.4 kDa), has a diameter of 3.2 nm [20]. Diffusion measurements in PLGA micro- and nanospheres encapsulating lysozymes involve pore sizes < 20 nm [9], so it was reasonable to describe diffusion in terms of individual random walks of molecules, rather than by transport of matter through surfaces. Experimental studies [9], have revealed that, in general, the initial pores have 5 - 80 nm in diameter, (proportional to the size of the encapsulated proteins). Equally, other experimental studies have reported cases of spheres with *initial occlusions* much larger than the Stokes-Einstein diameter of the microencapsulated molecule [3, 13]. Nevertheless, as long as the proteins undergo very restricted diffusion through pores, it is appropriate to treat diffusion by individual random walks of a given number of agents [21, 22]. In such cases, multi-agent systems seem reasonable approximations for a "protein - PLGA - pore" system.

The assumptions which apply to all models developed here are based on available experimental data [9]. The polymeric particles, modelled in 3D space, are considered to be completely spherical. The spheres are discretised throughout the volume into small sites. Figure 3 represents a schematic diagram of a section through a sphere during the simulation. The sites are seeded, according to predefined initial patterns, with elements such as PLGA polymer or protein

molecules. If necessary, an initial porosity value in the PLGA bulk material can be considered and, over time, more pores are formed.

The approach taken here to model the polymer erosion was based on Göpferich's theory for polymer erosion [16]. Events which occur independently with some average rate k are modelled by a Poisson process. It was assumed that the chain cleavage is a random event following Poisson kinetics. Considering that a site on the lattice erodes as a result of several Poisson processes which take place in parallel, the whole process is again a Poisson process. The waiting times t between k occurrences of the Poisson event are Erlang distributed.

$$f(t, k, \lambda) = \frac{\lambda^k t^{k-1} e^{-\lambda x}}{(k-1)!} \tag{1}$$

In Equation (1) k and λ are the shape and the rate parameters respectively. When $k=1$, the distribution becomes an exponential distribution for a positive variable, used to model the times *between* events that happen at a constant average rate:

$$f(t, \lambda) = \lambda e^{-\lambda t} \tag{2}$$

If the lifetimes of the sites are distributed according to Equation (2), then the mean lifetime of a single bond is given by $t = \frac{1}{\lambda}$.

In practice, the lifetime t can be computed using the following relation:

$$t = \frac{1}{\lambda} ln(U) \tag{3}$$

where U is a random number, uniformly distributed between 0 and 1 [16].

As dissolution proceeds, the lifetimes of the polymer sites begin to decrease. When a lifetime reaches zero the polymer from this site is considered eroded and the site becomes a pore. This approach permits the derivation of a relationship between real time and MC time through λ, the inverse of the mean lifetime of a PLGA particle, expressed in s^{-1}.

A protein molecule can leave its initial location only in the case where one of the neighbouring sites is a pore, (i.e. the molecules can only move through pores). Once in a porous channel, a molecule cannot leave it, except by escaping the sphere, when itis counted as dissolved. The internal configuration of the spheres in the model can be varied, depending on the internal morphology of the experimental spheres. In this way, the user can choose a model variant which addresses the problem most directly. Variants might be:

- homogeneous distribution of entities in the sphere
- stratified distribution of pores and/or concentrations of proteins
- structure with occlusions filled with proteins.

A more detailed description about modelling the internal morphology of the spheres is given in a parallel paper [23].
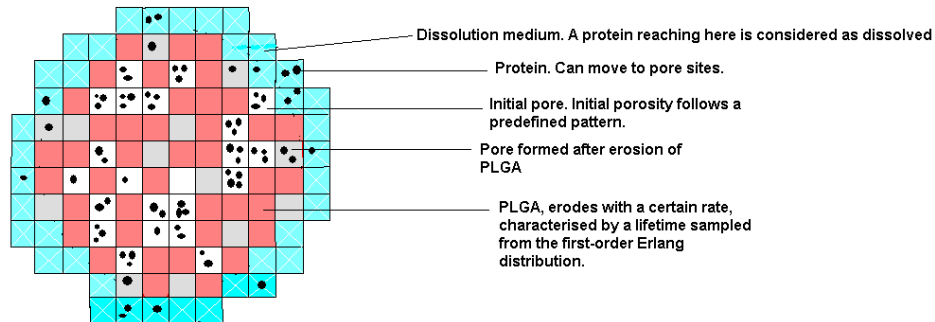

Fig. 3. Simplified scheme representing the main characteristics of the multi-agent model. Cross section through a 3D sphere.

3 Results and discussion

In this section, unless otherwise specified, the lifetimes of the PLGA particles were updated every 10 minutes, corresponding to the MC time-step, and samples were collected every 144 MC steps, (corresponding to one day). The number of particles per site was sampled from a uniform distribution between a lower and an upper value: $U(a1, a2), a1 < a2$. The Von Neumann neighbourhood was used.

3.1 Effect of Erosion Rate

Modern electron microscopy is able to provide information on pore formation [9, 13], therefore the rate of formation of pores of a certain size can be determined. The size of a site may be chosen to be in the dimensional range of the Stokes-Einstein protein diameter, or, for a coarser grained simulation, set equal to the average size of the initial pores. Thus, the mean lifetime of the sites depends on these initial assumptions and corresponding model choices. Figure 4, (a) represents the dynamics of porosity formation for spheres having a diameter of 80 sites and zero initial porosity. At every step, site lifetimes are decreased by Δt=10 minutes.

Clearly, lifetime influences the pattern of porosity dynamics, which is basically hyperbolic, but may be considered linear in the first 15-20 days. This agrees with [13], where porosity was found to grow linearly with time for the first 15 days of degradation of PLGA spheres. The figure shows that for λ=0.00002 min^{-1}, (i.e. $\frac{1}{\lambda}$=t=34 days) the porosity of the sphere increases from 0 to 0.8 over 55 days, (a typical experimental life-span of PLGA spheres). In this case, the pores appear quite quickly and result in a sponge-like topology of the system.
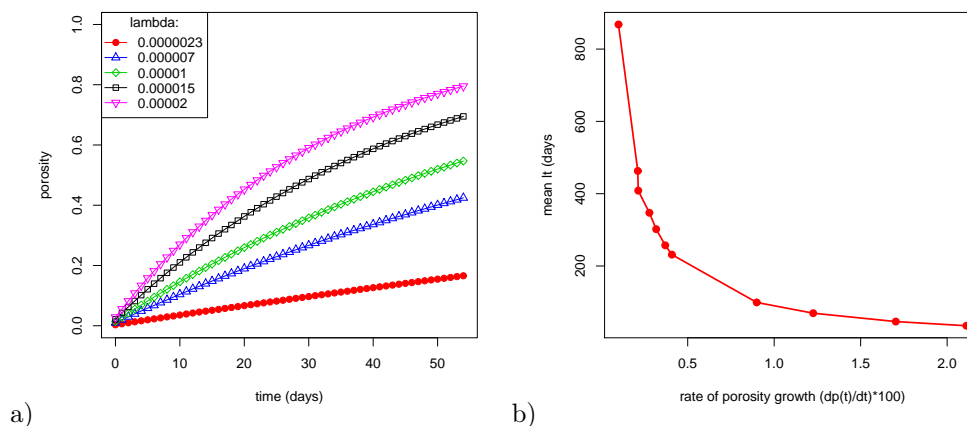
Fig. 4. a) Evolution of sphere porosity with time; porosity was computed using a zero-order Erlang distribution life-time approach b) Mean lifetime $\frac{1}{\lambda}$ used in MC simulations as a function of the porosity growth rate.

Figure 4, (b) represents an empirical relationship deduced between the parameter λ and the initial rate of pore formation. The rate was calculated using the linear part of the porosity dynamics curve (first 20 days). The authors suggest the idea, that if imaging techniques permit to identify the rate of porosity growth then Figure 4, (b) can be constructed for the needed sphere size and the parameter λ for quantitative simulations extrapolated.

Figure 5, shows how porosity growth dynamics can affect the release of molecules from a sphere. The same spheres used for obtaining Figure 4 have been seeded randomly with particles, having overall concentration $c = 0.02$. The release profiles obtained correspond to typical experimental profiles of release of macromolecules from PLGA spheres [9, 10]. In all cases, a short initial burst was observed, corresponding to the release of the particles situated on the surface of the sphere.

For each particle, the rate parameter, λ, affects the time during which it remains trapped in the PLGA. Thus, $t = \frac{1}{\lambda}$ is inversely proportional to the

rate of release of the molecules, mainly affecting the convexity of the release curve. With different lifetimes for the input, the model can generate profiles such as those found in [9, 10].
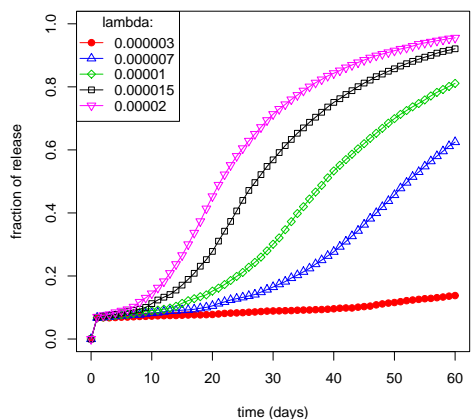

Fig. 5. Release profiles as a function of the degradation rate λ.

3.2 Effect of the distribution of drug particles in the sphere

We have verified the effect of initial loading on the emergent dissolution profiles. To do this, we have investigated the effects of the following two initial settings:

- the distribution of macromolecules per site on the dissolution profiles
- the initial protein loading

To examine the first case, the proportion of sites loaded with drug, was kept constant; while the number of particles per site was varied. For each run, $a2$ was increased. The particles released were considered in terms of *the fraction of the initial number of particles* in the sphere. Unexpectedly the simulations

predicted that as $a2$ increases, the fraction of the released drug does not significantly vary.

To examine the effect of the initial protein loading, the sphere loadings were considered in terms *of percentage of sites* on the lattice, containing one or more particles. Experimental work has shown that an increase in drug loading results in a corresponding increase in the release rate [9, 10]. Sandor et al. have measured the protein loadings, as a percentage of the total weight of the nanospheres. The values considered as low loadings were 0.5-1.6 % while high loadings of protein were 4.8-6.9 % [9]. Thus, to examine the effects of the initial loadings in a sensitivity analysis framework, concentrations close to experimental loadings were considered. Figure 6 shows the effect of the initial concentration on spheres having a diameter d=100 sites and mean lifetime $\frac{1}{\lambda}$ =69.4 days (λ=0.00001). *Again, no significant effect was evident from modification of the loading value, i.e. concentration appears to have no significant influence on the dissolution profiles.* Initially, this seems to be inconsistent with experiment, but, as shown in the following section, the shape of the dissolution profile, for all concentrations, is in fact given by *the initial porosity p.*

3.3 Initial porosity and initial macromolecular loading

In agreement with our simulations [9] suggest that the increase in the release rate at higher loadings actually occurs due to *initial porosity*: at low loadings (0.5 -1.6 %), small proteins seem to depend on diffusion through pores initially and on degradation at later times. Spheres with higher loadings are found to *have more interconnecting channels.* Sandor et al. consider the channels to be the reason why the higher-loaded spheres (4.8-6.9 %) do not exhibit the pronounced shift from diffusion-based to polymer erosion-based release seen with
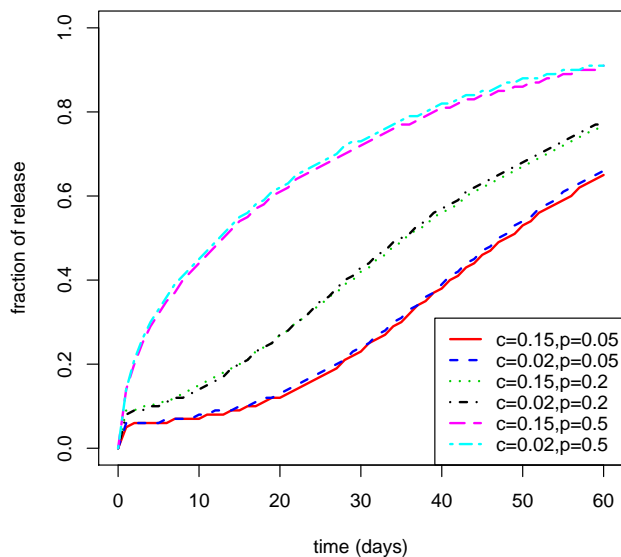
Fig. 6. For three different initial porosities, p_{01}=0.05, p_{02}=0.2, p_{03}=0.5, the dissolution profile was calculated using two values of the initial concentration, c_{01}=0.02 and c_{02}=0.15. Other model inputs: d=100, λ=0.00001, Δt=10 min, from 1 to 4 particles per site, (von Neumann neighbourhood).

the lower loaded spheres. Although [9] do not provide quantitative evidence of the increase in interconnecting pores and channels with initial protein loading, they clearly indicate that not only has the molecular weight of the protein an obvious effect on the initial porosity, (since larger proteins correlate to larger pores formed in the carrier spheres), but so has protein loading, (as larger loadings correlate with larger initial porosities). This supports our finding that the modifications in protein concentration influence the dissolution profiles only indirectly, by modifying the initial porosities of the PLGA-protein structures obtained. The authors suggest that quantitative studies, investigating how the protein loadings influence the structure of the final spheres, would help create better models for predictions in drug design.
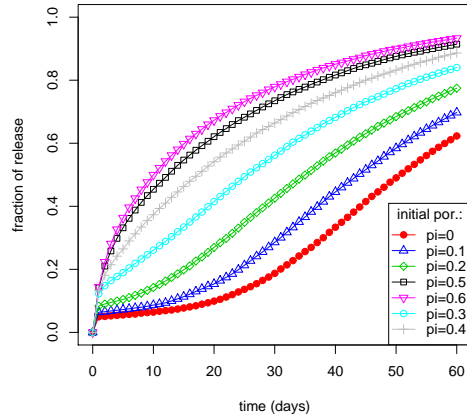
Fig. 7. Dissolution profile for different values of the initial porosity. Model inputs: d=100, λ=0.00001, Δt=10 min, c_0=0.02, from 1 to 4 particles per site, von Neumann neighbourhood.

Figure 7 shows the reaction to porosity modification for a sphere (d=100 and λ=0.00001), loaded with particles homogeneously distributed throughout its volume (c_0=0.02). As can be observed, even quite small variations of the initial porosity result in different dissolution profiles beginning with $\sim$ day 1 of dissolution.

There appears to be a threshold value for the initial porosity, p_{th}, which separates two different types of dissolution behavior. For $p<p_{th}$ two distinct dissolution phases can be observed, suggested by the change of shape (from convex to concave) of the release curve:

1. A first phase, corresponding to dissolution governed by diffusion through the initial pores.
2. A second phase where diffusion is generated by two processes: dissolution through the initial pores in conjunction with diffusion through pores created by the erosion process.

In the case of Figure 7, $p_{th} \approx 0.3$. The first phase ends around day 15. Between day 1 and day 15, the dissolution rate is constant and depends on the initial porosity. The second phase begins after day 15 and continues until the molecules are completely released from the spheres, around day 60. The dissolution profiles obtained for $p<0.3$ follow the same pattern as the lysozyme and the carbonic anhydrase at $\simeq 1.5\%$ initial loading from [9].

For $p_0 > p_{th}$, there no distinct phases of dissolution were observed. In Figure 7, for $p_{th} \approx 0.3$, the profiles obtained have a kinetic pattern as for lysozyme, $c_0=6\%$, alcohol dehydrogenase (1.1 % and 6.9 %) and thyroglobulin (0.5% and 4.8 %), from [9].

3.4 Quantitative discussion for the use of MC time step

One of the advantages of this work was cited as the fact that the protein dissolution in the heterogeneous porous environment of the PLGA spheres was taken into consideration *directly*, without passing through global parameters like the global porosity and the global tortuosity, in spite of knowing the structure of our spheres varies locally. However, working with a direct MC model brings the challenge of quantifying it.

The target of this section was to establish a relation between the diffusion coefficient of an encapsulated species in the matrix and the time interval Δt, determining the frequency that the model particles are updated.

In their article, Zhang et al. [14] mention two diffusivities: D_0 which is the solute diffusion coefficient in the solvent and D_{eff} the effective solute diffusion coefficient in the polymer matrix, depending on the internal morphology of the latter. Based on this work, the following empirical expression gives the effective diffusivity of a chemical species in a porous medium:

$$D_{eff} \sim \frac{D_0 p}{\tau} \qquad (4)$$

p is the porosity and τ is the dimensionless tortuosity of the medium. The porosity is one measure of the dimensions of the internal morphology, usually in the range 0.2-0.7 (fraction of volume) for polymers, [14]. As stated, the value of τ is usually between 1 and 100 for other pharmaceutical applications [14], but in the case of the PLGA τ reaches much larger values, in the range of $10^3 - 10^5$, because the drug molecule has to move through some narrow passageways which are produced by the vibrations of the polymer chain and control the actual pore size for the passage of macromolecules, [14].

To verify independently the value for the tortuosity, the literature for diffusion coefficients and effective diffusion coefficients experiments on PLGA spheres was examined. Batycky et al. [13] obtained the effective diffusivity of a protein in a PLGA medium: $D_{eff} = 2.00 \times 10^{-13}[cm^2/s] = 2.00 \times 10^{-17}[m^2/s]$. Goodhill [24] stated that $D_0 = 3 \times 10^{-7}[cm^2/s] = 3 \times 10^{-11}[m^2/s]$ for the diffusion coefficient of a protein of 17 kD (IL-1 beta). Zhang et al. [14] mention references which published $D_0 = 8.3 \times 10^{-11}[m^2/s]$ for BSA (bovine serum albumin). With these values of D_0, D_{eff} and p and Expression (4), the tortuosity τ indeed appears to be of the order of 10^5.

Fick's first law can be expressed as the following equation:

$$J = D\frac{dC}{dx}[kg/m^2 s] \ or \ [mol/m^2 s] \qquad (5)$$

where $dC = C_{sat} - 0$. Zhanf et al. [14] give C_{sat} in the range 1-100 $[kg/m^3]$. If the site of the sphere is Δx , then, for very small sizes of the site, such as 10 nm, the flux J is in the range of $10^{-8} - 10^{-7}[kg/m^2 s] = 10^{-26} - 10^{-25}[kg/nm^2 s]$. This quantity can be expressed as mass per surface of the site: $10^{-24} - 10^{-23}$ $[kg/site_-surface \times s]$.

Zhang et al. [14] give an example of concentration saturation $C_0 = 13.5[kg/m^3] = 13.5 * 10^{-27}[kg/nm^3] \simeq 10^{-24}[kg/site]$. Thus the time for a site of 10 nm to reach saturation is $t \simeq \frac{10^{-24}[kg/site]}{10^{-24}[kg/(site \times s)]} \simeq 1s$. This means that the time a site is occupied by a diffusing species is of the order of seconds. *In conclusion, choosing Δt for the model in the range of seconds should provide realistic simulations. The physical meaning of the time interval, during which the particles of the model move, is directly related to the mobility of the particles within the structure. In the case of a multi-agent model such as the present one, Δt does not completely reflect the diffusivity, but rather emerges in the effective diffusivity of the macromolecule, conditional on the pores of the device.*

Choosing much larger time-steps will slow down the release of the particles, whereas too small time steps will slow down the run-time of the model. Figure 8, (a, b, c) shows how choosing too large a Δt, such as 10 and 20 min, influences the dissolution profile, making it much slower. The effect of choosing Δt is especially visible when the sphere reaches percolation and the molecules gain mobility.

Spheres have porosity organised in 3 strata, with value decreasing from the mantle to the core. The simulation indicates more clearly the mechanisms behind the dissolution profiles. The smaller Δt is, the more frequently the particle may update, i.e. move to a neighbouring site with specified probability. Figure 8, (a, b, c), (t>20 days), shows that in the case where the environment permits mobility, (right hand side of the graphs), different values for Δt can considerably change the rate of dissolution profile.

Figure 8, (a) is a particularly good example: the spheres started at zero initial porosity, but a small initial burst of particles released can still be observed. Further, porosity was allowed to increase slowly, (λ=0.00001). At day 16, when the value of the porosity reaches the threshold value of p_{th}=0.2, the

profiles split according to the different values of Δt used, and clusters of pores spanning the whole sphere begin forming at this point in time.

Figures 8, (b) and (c), show release behaviours in steps, due to the sequential percolation through the three strata by connected pores. The first stratum is initially percolated and is the origin of the initial burst. The second stratum is apparently percolated very quickly after dissolution begins, (before day 10), while the stage, which can be observed by day 20, is caused by a spanning cluster of pores formed in the last stratum.
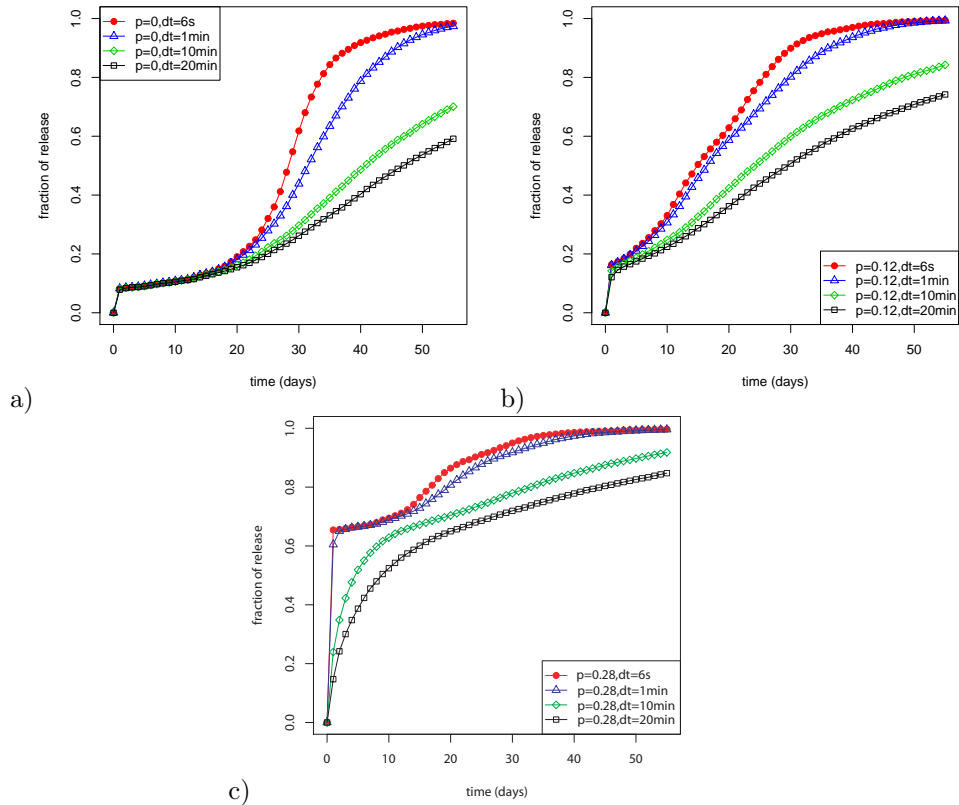

Fig. 8. Effect of the time step Δt used to perform the updating in the simulation.

4 Validation with experimental data for quantitative measurements

Table 1 presents a list of variables, the values of which need to be determined in order to perform a simulation aiming validation of a model version (several versions are available for a number of internal configurations of the spheres [23]), or prediction of the dissolution profile in a given experimental situation. However, the value of this modelling work is that the framework, once developed, complements situations, where accurate experimentation is difficult, since it enables postulation of plausible system values and analysis outcome over a range, as in the situation of lysozyme release presented in the following: The experimental data set referred to here is due to [9] and it relates to

Table 1. Quantities needed for the simulation of protein dissolution from microspheres

Description	Variable
Size of the sphere	d
Effective diffusivity/mobility of the macromolecules through the pores	D_{eff}
Diffusivity of the macromolecules in the solvent	D_0
Diameter of the macromolecules	a
Sphere loading	c
Concentration of the macromolecule at different depths of the sphere	c_{01}, c_{02}, c_{03}
Size of the pore one wish to consider	p_d
Initial porosity	p_0
Pattern of repartition of pores in the volume of the sphere	p_{01}, p_{02}, p_{03}
Rate of pore formation	λ

a set of nanospheres, encapsulating the lysozyme, a very small protein. The spheres have been analysed by electron microscopy and they appear compact and non-porous. This means that the pores, if these exist, have diameter $<$ 20 nm (i.e. below the resolution levels of the microscopy technique [9]). In the simulations, spheres with no initial pores, as well as spheres with very small

Table 2. Properties of nanospheres loaded with lysozyme; corresponding modelling choices taken after evaluation of this data

Variable	Value	Model
d	200-250 nm	50 sites
D_{eff}	N/A	Δt =10min, 1min and 6 sec
D_0	N/A	not needed here
a	$\simeq$3 nm	-
c_0	1.6% and 6.9% of total weight	c_{0low} =0.016 and c_{0high} =0.069
$c_{01}/c_{02}/c_{03}$	N/A	c_0 /0.5c_0/0.2c_0
p_d	>20 nm	5 nm/site
p_0	N/A	p_{0low} =0 and p_{0high} =0.3
$p_{01}/p_{02}/p_{03}$	N/A	p_0 /0.3p_0 /0
λ	N/A	5×10^{-6}

pores of 5 nm in diameter, just above the Stokes-Einstein diameter of the lysozyme (3 nm), were considered. Given that the diameter of a site is equal to the diameter of a pore p_d, and the diameter of the sphere is d, the average size of the sphere is 50 sites. The λ parameter was chosen to be $5 \times 10^{-6} s^{-1}$, corresponding to a total 55 days of dissolution. Three different values of Δt have been used. It turned out that the non-porous sphere does not generate a dissolution profile characterised by the significant initial burst, observed experimentally. The best results were obtained with the porous sphere using the smallest time step: Δt=6 s (as predicted in the previous section). In Figure 9, (a), the points indicating a slow release experimental curve correspond to an initial loading of 1.6%, while the curve of very fast release has been obtained in [9] with an initial loading of 6.9%.

Other slightly larger nanospheres, encapsulating larger proteins, were examined in the work of Sandor et al. [9] and they were found to have stratified porosities - larger pores in the mantle and smaller at the core. This is why it was decided to perform simulations with homogeneous porosity on one hand and stratified porosities with different configurations of the strata, on the

other hand. Table 2 shows the best performing strata configuration, as well as the values for other measured or estimated parameters.

Figure 9, (b) illustrates performance of the model calibrated to simulate release of carbonic anhydrase from microspheres of size $\simeq 1$ μm, described, like previous spheres, in [9]. More details on this example are available in [23], which focuses on the importance of correctly modelling the internal morphologies of PLGA spheres.
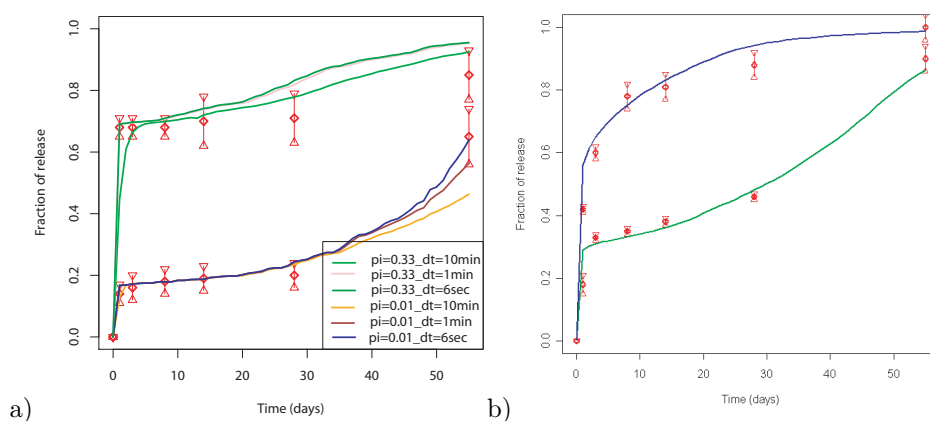

a)   b)

Fig. 9.   a)Experimental lyzosyme release versus simulated drug release from biodegradable microspheres. Red rhombi represent the experimental points from Sandor et al. [9]. Continuous curves show simulated results obtained with different Δt values. b) Experimental carbonic anhydrase versus simulated drug release from biodegradable microspheres. Red rhombi represent experimental points [9]. Continuous curves show simulated results obtained with different Δt values.

5 Conclusion

This paper presents an exploratory framework for modelling dissolution of proteins from PLGA microspheres. It has been shown that the initial model can be modified to simulate a number of experimental situations. For the

PLGA microspheres, the results obtained in the work presented above are in good agreement with experimental work [9]. The models developed can be easily used to simulate other cases of protein dissolution from PLGA microspheres. Finally, the multi-agent approach permits in-depth exploration of the problem. Building on the nested levels of complexity in the multi-agent system, in a step-by-step way and comparing the results obtained by simulation, permits the testing of different hypotheses about the system or can be used to confirm recent experimental work on the inner configuration of the spheres.

References

[1] Ungaro, F., Biondi, M., Indolfi, L., Rosa, G. D., Rotonda, M. I. L., Quaglia, F. and Netti, P. V Biomaterials (2004).

[2] Merkle, H., Gander, B., Meinel, L. and Walter, E. Business Briefing: Pharmatech. (2002) 1–6.

[3] Charlton, D., Peterson, M., Spiller, K., Lowman, A., Torzilli, P. and Maher, S. A. Private communication (2006).

[4] Göpferich, A. American Inst. of Chem. Eng. (AIChE) Journal 41(10) (1995) 2292–2299.

[5] Feng, S. and Chien, S. Chemical Engineering Science 58 (2003) 4087–4114.

[6] ul Ain, Q., Sharma, S. and Khuller, G. K. Antimicrobial Agents and Chemotherapy 47(9) (2003) 3005–3007.

[7] Illum, L., Church, A., Butterworth, M., Arien, A., Whetstone, J. and Davis, S. Pharm. Research 18(5) (2001) 640–645.

[8] Kilic, A. C., Capan, Y., Vural, I., Gursoy, R. N., Dalkara, T., Cuine, A. and Hincal, A. A. J. Microencapsulation 22(6) (2005) 633–641.

[9] Sandor, M., Enscore, D., Weston, P. and Mathiowitz, E. J. Controlled Release 76 (2001) 297–311.

[10] Lam, X., Duenas, E., Daugherty, A., Levin, N. and Cleland, J. J. Controlled Release 67 (2000) 281–292.

[11] Siepmann, J. and Göpferich, A. Advanced Drug Delivery Reviews 48 (2001) 229–247.

[12] Siepmann, J., Faisant, N. and Benoit, J.-P. Pharm. Research 19(12), (2002) 1885–1893.

[13] Batycky, R. P., Hanes, J., Langer, R. and Edwards, D. A. J. Pharm. Sci. 12 (1997) 1464–1477.

[14] Zhang, M., Yang, Z., Chow, L.-L. and Wang, C.-H. J. Pharm. Sci. 92(10) (2003) 2040–2056.

[15] Göpferich, A. Biomaterials 17 (1996a) 103–114.

[16] Göpferich, A. Biomaterials 18 (1997b) 397–403.

[17] Göpferich, A. J. Controlled Release 44 (1997a) 271–281.

[18] Zygourakis, K. and Markenscoff, P. A. Biomaterials 17 (1996) 125–135.

[19] Zhao, A. and Rodgers, V. J. Controlled Release 113(12) (2006) 15–22.

[20] Kisler, J. M., Stevens, G. W. and O'Connor, A. J. Materials Physics and Mechanics 4 (2001) 89–93.

[21] Kosmidis, K., Rinaki, E., Argyrakis, P. and Macheras, P. Int. J. Pharm. 254(2) (2003b) 183–188.

[22] Nicholson, C. and Sychova, E. Trends in Neurosciences 21(5) (1998) 207–215.

[23] Barat, A., Ruskin, H. J. and Crane, M. Theory in Biosciences, Special Issue, In Press (2007).

[24] Goodhill, J. Eur. J. Neurosci. 9 (1997) 1414–1421.